Michel, S. E. S., Rogers, S. E., Briscoe, W. H., & Galan, M. C. (2020). Tuneable Thiol-Ene Photo-Crosslinked Chitosan-Based Hydrogels for Biomedical Applications. *ACS Applied Bio Materials*, *3*, 8075-8083. [11]. https://doi.org/10.1021/acsabm.0c01171

Tuneable Thiol-Ene Photo-Crosslinked Chitosan-Based Hydrogels for Biomedical Applications

Sarah E.S Michel[†], Sarah E. Rogers[§], Wuge H. Briscoe[†*], M. Carmen Galan[†*]

[†] School of Chemistry, University of Bristol, Cantock's Close, Bristol BS8 1TS, UK
[§] ISIS Neutron and Muon Source, Science and Technology Facilities Council, Rutherford Appleton Laboratory, Didcot, OX11 0QX, UK

Abstract: Access to biocompatible hydrogels with tuneable properties is of great interest in biomedical applications. Here we report the synthesis and characterisation of a series of photo-crosslinked chitosan hydrogels from norbornene-functionalised chitosan (CS-nb) and various thiolated crosslinkers. The resulting materials were characterised by NMR, swelling ratio, rheology, SEM and small angle neutron scattering (SANS) measurements. The hydrogels exhibited pH- and salt-dependent swelling, whilst the macro- and micro-scale properties could be modulated by the choice and degree of crosslinker or the polymer concentration. The materials could be moulded *in situ* and loaded with small molecules that can be released overtime. Moreover, the incorporation of collagen in the hydrogels drastically improved cell adhesion, with excellent viabilities of human dermofibroblast cells on the hydrogels observed for up to 6 days, highlighting the potential use of these materials in the biomedical area.

KEYWORDS: polysaccharides, hydrogels, chitosan, biocompatible materials, thiol-ene, photocrosslinking

Introduction

Hydrogels are defined as physically or chemically crosslinked hydrophilic polymer chains swollen in water. Owing to their swollen 3D structure, they constitute an excellent mimic of human tissues and provide an appropriate scaffold for cells to grow on and have been therefore widely exploited in the fields of wound healing and tissue engineering.[1-3,4,5]

A wide range of natural as well as synthetic and hybrid polymers have been used to produce hydrogels via chemical or physical crosslinking. In this context, polysaccharides are highly attractive hydrogel precursors for biomedical applications as they are inexpensive and abundant yet biocompatible, biodegradable and bioactive materials owing to the similarities with glycosaminoglycans (GAG) and glycoproteins found in the extracellular matrix (ECM). Moreover, polysaccharides contain multiple functional groups of different reactivities enabling

their tailored functionalisation and crosslinking.[6-8] Chitosan (CS) is the only cationic natural polysaccharide consisting of β-1,4-D-glucosamine (GlcNAc) and β-1,4-N-acetyl-D-glucosamine (GlcNAc) units. CS is generally obtained by deacetylation of at least 50 % of GlcNAc residues of chitin.[9] The presence of free amines imparts CS with mucoadhesion properties, hemostatic action and antibacterial activity, while its similarities with GAGs provide a favourable environment for cell adhesion or proliferation.[10-14] CS has shown particularly promising applications in wound healing and tissue engineering as CS-based materials allow for efficient delivery of fragile bioactives such as growth factors or proteins.[8, 10, 12, 15, 16] In addition to wound healing applications, CS alone enhances vascularisation and reduces scaring. It has also been shown to support attachment and proliferation of various cell lines such as fibroblasts, nerve cells or chondrocytes.[17-19]

Chemically photo-crosslinked CS-based hydrogels provide an extra spatio-temporal control over hydrogel formation through the positioning of the light source. CS photo-crosslinkable precursors are typically obtained by (meth)acrylation, leading to random gel network formation.[20] Alternatively, the thiol-ene photo-click reaction using norbornene (nb) as the bicyclic strained alkene partner has many advantages since nb is highly stable under physiological conditions, yet highly reactive towards radicals driven by the strain release from an sp^2 alkene to an sp^3 alkane.[21, 22] The coupling reaction proceeds with fast kinetics with various long-wavelength UV (Irgacure 2959[23] – IRG) or visible-light activated photoinitiators (Eosin Y[24] or riboflavin[25]).

We previously reported the synthesis of novel biocompatible CS-based microgels obtained through thiol-ene photoclick crosslinking of CS-hydrogel precursors bearing a norbornene moiety (CS-nb, **Figure 1**).[26, 27] This precursor, obtained in a single step by ring-opening of cheap and commercially available carbic anhydride, presented improved water solubility compared to native CS, which was attributed to the concomitant introduction of a carboxylate moiety acting as a solubilising group. In the current study, we investigate the physical properties of a series of CS-nb hydrogels using three different thiol-based crosslinkers. We show that the structure and physicochemical properties of the hydrogels can be modulated by the choice of photo-crosslinker, which in turns affects cell adhesion and proliferation depending on the chosen cell line. The cytocompatibility and potential biomedical applicability was finally investigated.

Results and discussion

For a minimum CS concentration of 1 w:v%, hydrogels employing CS-nb as the starting material were generated within seconds in all cases under UV-A, with Irgacure (IRG) as photoinitiator[26] and using three different cross-linkers: a short and a long thiolated PEG derivative (namely HS-PEG$_2$-SH and HS-PEG$_{40}$-SH with to the subscripts denoting the number of ethylene glycol repeat units), and a thiolated CS (CS-SH) synthesized by ring-opening of Traut's reagent[28], respectively (see **Figure 1** for chemical structures). It was proposed that the final properties of CS-nb hydrogels would be influenced by the nature of the crosslinker structure. For instance, CS-SH present multiple thiol functionalities close to the CS backbone which are randomly located along the CS polymer chain, whereas both thiolated PEG derivatives are bifunctional and linear. The greater mobility provided by HS-PEG$_{40}$-SH after crosslinking was anticipated to increase the hydrogels elasticity compared to the shorter variant HS-PEG$_2$-SH.

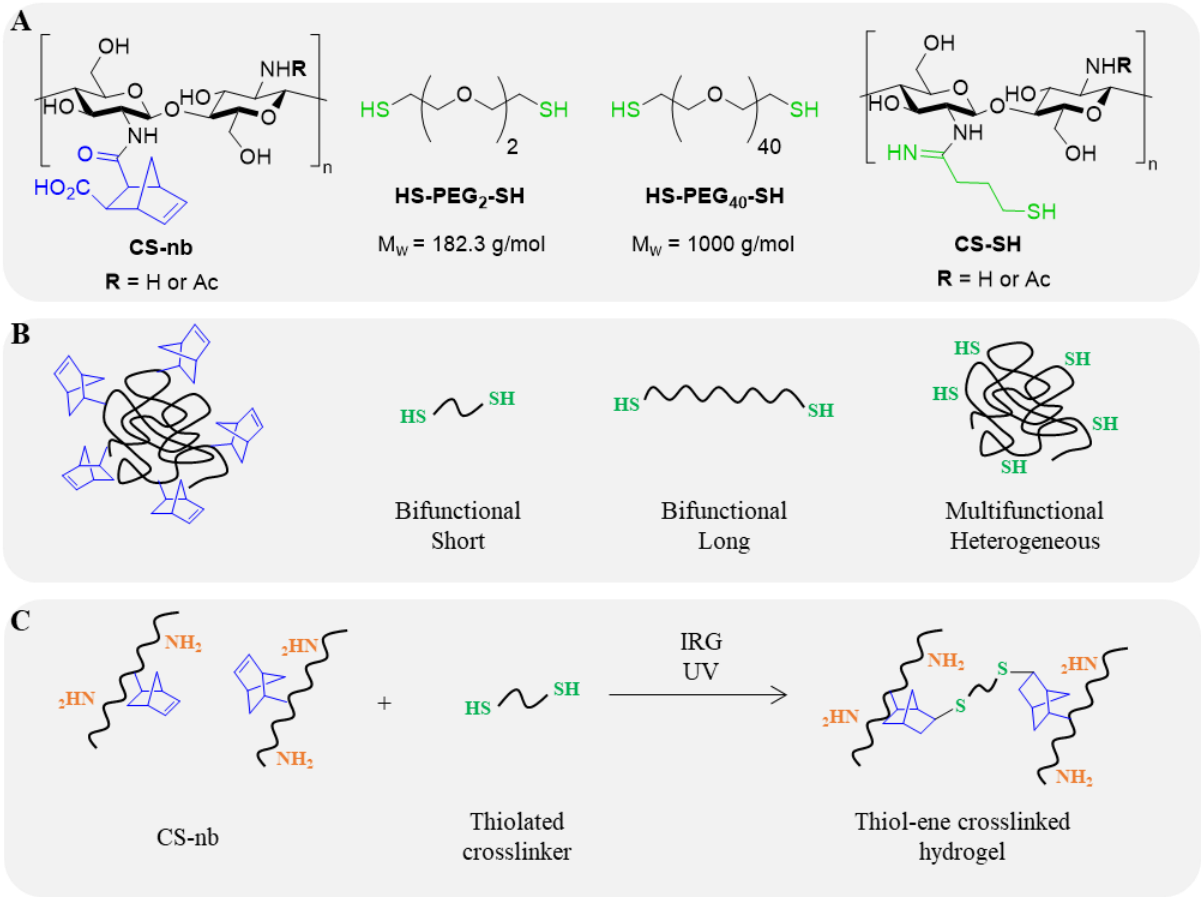

Figure 1. Chemical structures and abbreviations of nb-functionalised CS and three thiolated crosslinkers used in this work (A). Schematic representation of the polymers and crosslinkers involved and the key parameters studied in the hydrogel properties (B). Hydrogel formation mechanism through thiol-ene photoclick chemistry (C).

Subsequently, the physicochemical properties of the different hydrogels were evaluated. Interestingly, as a weak basic polyelectrolyte, CS hydrogels can exhibit both pH- and salt-induced swelling.[29, 30] For a fixed CS concentration (2 w:v%) and [SH]:[nb] molar ratio R_s = 1:1, the maximum swelling ratio (SR) was obtained under acidic conditions (SR ~ 55) where amines were fully protonated and repel each other. Significant shrinkage was observed under basic conditions or in the presence of salts (SR ~ 10-20), as expected from the neutralisation of the polymer chains (**Table 1**). Polyelectrolyte conformational shrinkage generally occurs in the presence of salts due to ionic screening of the electrostatic interactions between polymer chains.[31] CS-SH crosslinked hydrogels presented lower and less reproducible SR, possibly due to a more heterogeneous crosslinking. SR was slightly higher for hydrogels crosslinked with HS-PEG_{40}-SH (SR ~ 65), which was the longest and more flexible crosslinker, thus allowing for greater mobility between polymer chains and hence higher water uptake.

Table 1. Swelling ratios (SRs) of 2% CS-nb hydrogels in different solution conditions depending on the crosslinker.

	DI water	**pH = 3**	**pH = 11**	**PBS**
HS-PEG_2-SH	54.3 ± 5.4	64.4 ± 11	15.3 ± 5.7	12.9 ± 0.43
HS-PEG_{40}-SH	64.5 ± 4.4	54.5 ± 4.8	16.4 ± 1.4	19.3 ± 0.79
CS-SH	45.9 ± 16.3	54.9 ± 17	11.0 ± 2.4	9.0 ± 0.77

Following freeze-drying, all hydrogels presented similar honeycomb-like structures with highly polydisperse pores of dimensions varying between d ~ 20 and up to ~ 120 µm, evident from SEM images (**Figure 2**). It is worth noting that SEM required preliminary drying of the samples, which might affect the actual structure of the hydrogels. As anticipated, smaller pores were observed for HS-PEG_2-SH (d ~ 33 ± 10 µm) than for HS-PEG_{40}-SH-crosslinked materials (d ~ 45 ± 15 µm). The pore size of the hydrogels employing CS-SH as the crosslinker was more polydisperse, with both small pores of d ~ 30 µm and also more open structures of d ~ 60-90 µm observed.

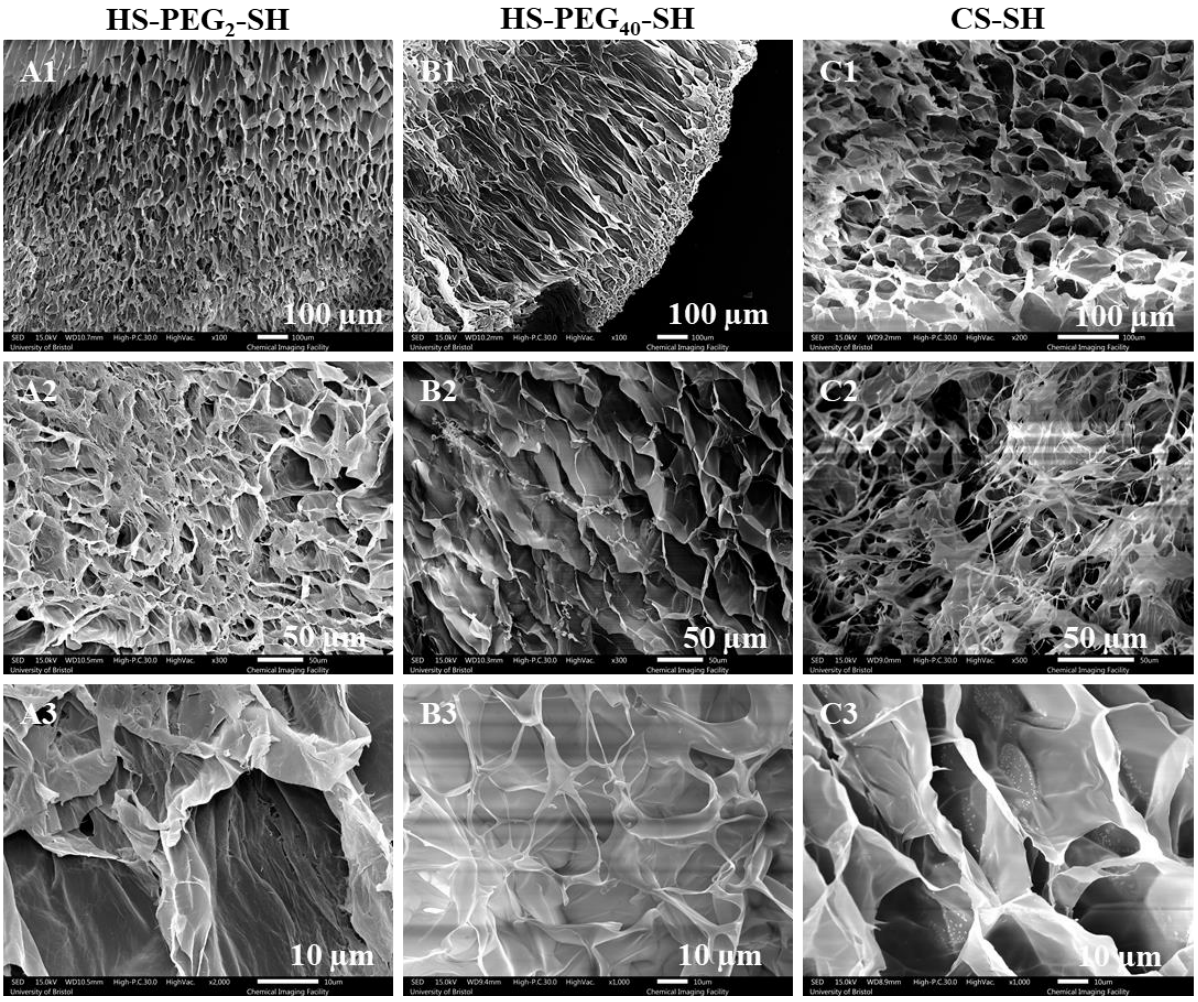

Figure 2. SEM images under different magnifications of CS-nb hydrogels crosslinked with: HS-PEG_2-SH (A1-3), HS-PEG_{40}-SH (B1-3) and CS-SH (C1-3).

All the materials showed the rheological properties characteristic of viscoelastic covalent hydrogels: the storage modulus *G'* was at least 10 times higher than the loss modulus G'', and all the samples presented negligible frequency-dependency (**Figure 3** and **Figures S2-S5**). The rheological properties of all the hydrogels were highly dependent on the crosslinking density and the polymer concentration, with higher degree of crosslinking and polymer concentration yielding greater *G*' modulus (varying from ~ 0.02 to ~ 20 kPa), which is consistent with previous reports. [32-34] Hydrogels crosslinked with the shorter HS-PEG_2-SH presented *G*' modulus up to 10 times greater than those crosslinked with longer HS-PEG_{40}-SH or CS-SH. The crosslinker length can directly impact on how tightly the polymer chains are packed together in the gel: the shorter the distance between crosslinking points, the lower the chain mobility and therefore the greater the solid-like behaviour, as reflected by an increase in *G*'. HS-PEG_{40}-SH is both longer and more flexible, allowing for more polymer chain

rearrangement under shear. CS-SH should therefore present very tightly packed networks due to the high thiol density per polymer chain. The lower *G*' values suggest either incomplete crosslinking, possibly due to the random thiol localisation and their proximity to CS backbone which reduced their availability, or a more heterogeneous structure, consistent with the random thiol localisation along the chain.

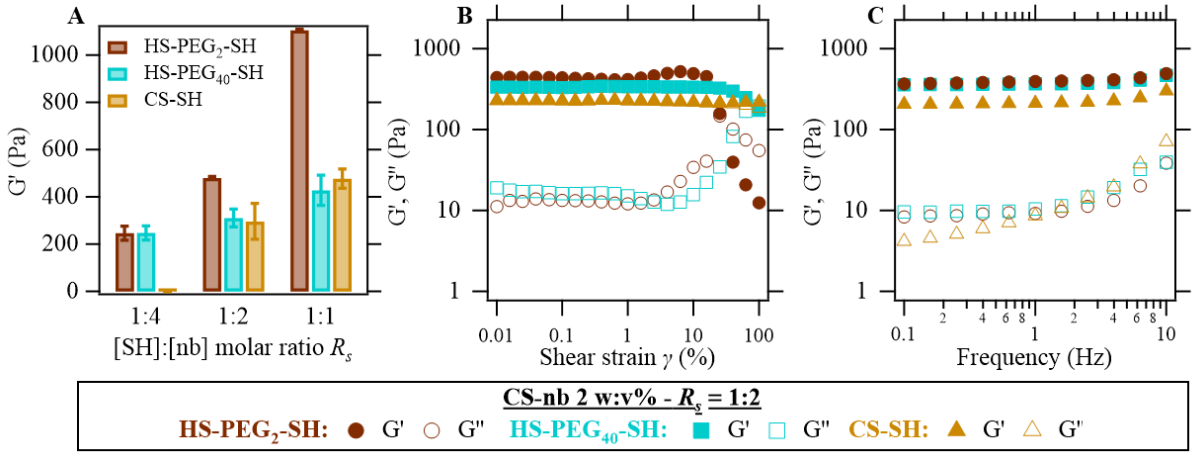

Figure 3. Rheological properties of 2 w:v% CS-nb hydrogels using different crosslinkers. (A) Averaged *G*' and *G*'' on the linear viscoelastic region determined by amplitude sweep measurements for various crosslinkers and [SH]:[nb] molar ratios R_s. *G*' and *G*'' from (B) amplitude sweep at a shear frequency of 1 Hz and (C) frequency sweep measurements at a strain rate of γ = 1% of 2% w:v CS-nb hydrogels crosslinked for R_s = 1:2.

The effect of the crosslinker on the internal structure of the hydrogels was further investigated using SANS. The formation of crosslinking points was evidenced by the linear increase in the scattering intensity *I* at low *q*, related to the formation of large structures (**Figure 4**). This increase was characterized by a mass fractal of ~ 2.4 – 2.6 consistent with the formation of a crosslinked network (

Table 2 and **Table 3**). The scattering of hydrogels can be generally described by the combination of a liquid-like ($I_L(q)$) and a solid-like ($I_S(q)$) scattering terms modelling the polymer chain in solution and the crosslinking points respectively:

$$I_{gel}(q) = I_L(q) + I_S(q) \quad (1)$$

The polymer contribution $I_L(q)$ is usually given by a Lorentzian equation:

$$I_L(q) = \frac{I_L(0)}{1+\xi^2 q^2} \quad (2)$$

The solid-like contribution arises from heterogeneous crosslinking, leading to densely and poorly reticulated areas.[35] These inhomogeneities are typically described by one of the

following functions: a Gaussian term, an exponential function, or the Debye-Buesche-Anderson (DAB) model.[35, 36]

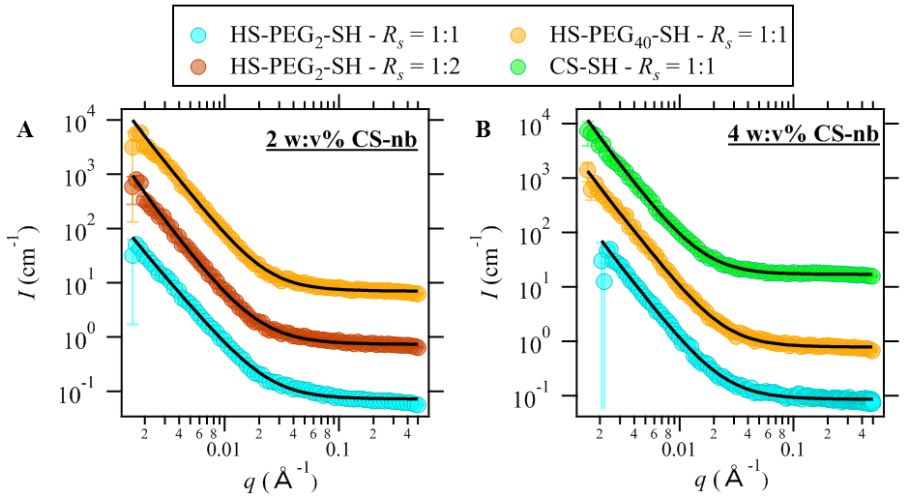

Figure 4. SANS data of CS-nb hydrogels using different crosslinkers at different CS-nb concentrations: (A) 2 w:v% and (B) 4 w:v%. Fitted data are shown as a black line. Data have been offset (by a factor of 10 sequentially) on the y-axis for clarity.

Hammouda *et al.* investigated the poly(ethylene oxide) (PEO) clustering mechanism leading to gel formation. The system was well modelled by the addition of a Lorentzian equation describing the polymer chain scattering and a Porod scattering term representing the clusters:[37]

$$I(q) = \frac{A}{q^D} + \frac{C}{1+(q\xi)^m} + B \qquad (3)$$

where D is the Porod exponent of the system, m is the Lorentzian exponent, ξ is the correlation length and A, C and the background B are all constant. The Lorentzian exponent is related to the polymer-solvent interactions, with $m < 2$ characteristic of efficient polymer solvation and $m > 2$ typically representative of polymer chains in a θ solvent. This model was successfully applied by Saffer *et al.* in their study of photo-chemically crosslinked PEG hydrogels through thiol-ene chemistry, a chemically similar system to ours.[38] In addition, the introduction of the exponent m in the Lorentzian term account for hydrogen bond rich networks, frequently occurring in polysaccharide-based hydrogels, for which a deviation in $I_L(q)$ has been observed.[39]

This equation described very well the scattering of the CS-nb hydrogels (**Figure 4**). As the baseline was not flat, the background scattering value B was fixed by fitting the high/intermediate q region to a power law as described by Saffer *et al.*:[38]

$$I(q) = \frac{A}{q^D} + B \quad (4)$$

The correlation or mesh size obtained with Eq. 3 for 2 w:v% hydrogels compares very well with those obtained by rheology, calculated with Eq. S3 (**Table 2**). As the degree of crosslinking increases from R_s = 1:2 to 1:1 the mesh size ξ decreases from ~ 29 to ~ 20 nm, consistent with more crosslinking points bringing the polymer chains in closer proximity. The use of a longer crosslinker led to bigger ξ (19 to 27 nm) as expected. The Porod exponent, D = 2 - 3, is consistent with hydrogel formation, while the Lorentzian exponent m is lower than 2, indicating that the polymer chains behaved as in a good solvent.[38]

The values of the mesh size obtained from SANS fitting for the 4 w:v% hydrogels differ from those obtained by rheology, especially for HS-PEG_2-SH and CS-SH hydrogels (**Table 3**). The general trend of ξ increasing from HS-PEG_2-SH to HS-PEG_{40}-SH is still verified. The smallest mesh size was measured for CS-SH hydrogels with SANS (ξ = 11 nm) while a bigger mesh size (ξ = 17 nm) was obtained from the G' value. Hyland *et al*. observed very different ξ values obtained from rheological and SANS measurements, suggesting that the material mechanical properties were not only a result of the network density – measured as the correlation length L_c using the DAB model – but also of the fiber thickness and its packing.[40] Rheology measurements also probe macroscopic properties, while SANS probes the nanostructure of the polymer network. Due to the high thiol content of CS-SH and its proximity to the polymer backbone, it is likely that these hydrogels were very heterogeneous, with highly reticulated area where the thiols could be accessed and sterically hindered regions which remained uncrosslinked. The access to a smaller q range in further SANS measurements would provide more information on the dimension of the resulting aggregates.

Table 2. Summary of rheology and SANS characterisation results of 2w:v% CS-nb hydrogels. Rheology, ρ_s: crosslinking density; ξ: mesh size, calculated from Eq. S3 and S4, respectively. SANS, D: fractal dimension; m: Lorentzian exponent in Eq. 3.

Hydrogel		**Rheology**			**SANS**			
R_s	**Crosslinker**	G' (Pa)	ρ_s (mol/m^3)	ξ_a (nm)	ξ (nm)	D	m	χ^2
1:1	HS-PEG_2-SH	1107	1.17	19.2	18.4 ± 3.5	2.43	1.43	3.65
1:2	HS-PEG_2-SH	479	0.19	25.5	29.3 ± 2.3	2.79	1.58	3.98

1:1	HS-PEG$_{40}$-SH	435	0.18	26.2	27.9 ± 4.9	2.60	1.37	3.59
1:1	CS-SH	477	0.19	25.5	-	-	-	-

Table 3. Summary of rheology and SANS characterisation results of 4w:v% CS-nb hydrogels. Rheology, ρ_s: crosslinking density; ξ: mesh size, calculated from Eq. S3 and S4, respectively. SANS, *D*: fractal dimension; *m*: Lorentzian exponent in Eq. 3.

Hydrogel		**Rheology**			**SANS**			
R_s	**Crosslinker**	G' (Pa)	ρ_s (mol/m^3)	ξ_a (nm)	ξ (nm)	D	m	χ^2
1:1	HS-PEG$_2$-SH	11560	4.67	8.79	15.2 ± 0.3	2.61	1.43	1.49
1:1	HS-PEG$_{40}$-SH	1695	0.67	16.8	20.0 ± 4.7	2.60	1.42	1.83
1:1	CS-SH	1535	0.67	17.2	11.3 ± 0.7	2.73	1.95	4.37

The fractal dimension *D* is also relevant to biological applications of hydrogels, as shown by Hung *et al.* on agarose physical hydrogels. They synthesized a variety of hydrogels of matching rheological properties but different mass fractals measured by both rheology and SAXS. While the impact of rheology on cell culture is well-known, they were the first to observe that the hydrogel fractal dimension also had a significant impact on stem cell differentiation.[41] CS-nb hydrogels studied here with SANS presented very similar mass fractals $D \sim 2.6$, suggesting that we can correlate the hydrogel rheological properties directly to their behaviour with cells, as we show below. In addition, the range of achieved shear modulus (G' = 0.020-20 kPa) was relevant to a wide area of biomedical applications, ranging from neural tissue engineering (~ 100 Pa) to muscle or skin cell culture (~ 10 kPa).[42]

CS-nb hydrogels of tailored shapes could be easily obtained using moulds (**Figure 5A**). To demonstrate the ability of our hydrogels to encapsulate and slowly release molecules over time, fluorescent dye rhodamine B was used as a model compound and entrapped within the hydrogel structure during the gelation process. After one week of immersion in water, the gel had swollen and lost most of its colour due to rhodamine release. Although the rate of release was not quantified, this highlights the possible application of these hydrogels for drug delivery, especially due to their improved swelling properties under acidic conditions, which is a common feature of tumours and infected organs, an area under our current investigation.

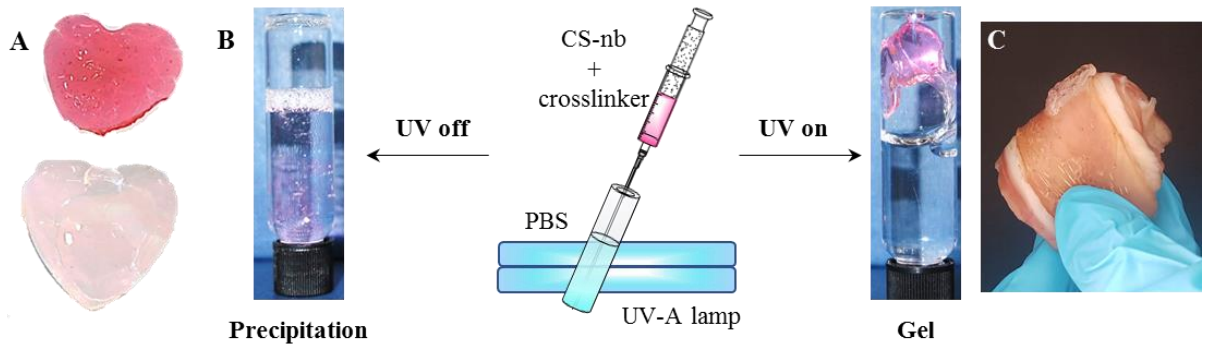

Figure 5. Potential CS-nb hydrogel applications. (A) Drug-release: shape-retaining heart with encapsulated rhodamine as generated (top) and after one week of storage in water (bottom). (B) *In-situ* generated hydrogels in PBS. (C) Hydrogel adhesion on pork skin (*in situ*-synthesised).

Owing to the very fast gelation kinetics, hydrogels could be generated *in situ* when the liquid polymer precursor was injected in PBS under UV, independently of the crosslinker used (R_s = 1:1). It is important to note that if the UV source was switched off, CS precipitation, instead of gelation, occurred upon injection due to its low solubility under physiological conditions. (**Figure 5B**). Hydrogels could also be generated *in situ* directly on pork skin, both in dry state and in PBS, and gel adhesion was observed on the skin that was stored in PBS for up to 4 days (**Figure 5B,C**), suggesting potential applications in wound healing. The adhesion was most likely due to the generation of free radicals in the initiation step which could recombine with functional groups present on the skin.[43, 44] CS-nb precursor solutions containing IRG could also be sterilised in an autoclave before triggering the gelation with UV, since no structural change were observed on the precursors solution by ^{1}H NMR.

Hydrogels have been widely studied for cell culture as they provide a 3D structure for cells to grow and develop which is similar to human tissues.[45] Substrates favouring skin wound healing and fibroblast growth frequently present G' ~ 0.5 – 10 kPa,[46-48] which informed the choice of hydrogels for initial toxicity testing (3 crosslinkers at either 2 or 4 w:v%, R_s = 1:1), which covered a wide range of rheology and swelling properties. A good hydrogel candidate for a tissue engineering approach must allow cells to adhere, infiltrate and spread in the scaffold; failing to do this will lead to cell toxicity, which can be assessed by metabolic activity measurements or live cell fluorescent staining. Human skin fibroblasts (HDF), a standard model for wound healing and tissue engineering applications, and placenta choriocarcinoma cells (BeWo-b33), an established model of the placental membrane[49] and relevant to wound healing as an epithelial monolayer, were cultured on top of the six different chosen hydrogels.

Both cell lines presented limited adhesion on the gel substrate, with better spreading for BeWo on softer gels (2 w:v%) and for HDF on stiffer gels (4 w:v%), while cell aggregates where observed on the softest substrates, indicating unsuccessful adhesion and consequent cell death (**Figure 6**). The metabolic activity as measured using Alamar Blue (AB) reagent was between 60 and 80 % for BeWo compared to ~ 20 – 35 % for HDF on the softest substrates (2 w:v%) , which increased up to 80 % on the 4 w:v% hydrogels (**Figure 6**). The observed stiffness-spreading relationship of HDF is consistent with previous work on non-biofunctionalised acrylate hydrogels – *i.e.* without the introduction of peptides or sugars to impact on adhesion.[50, 51]

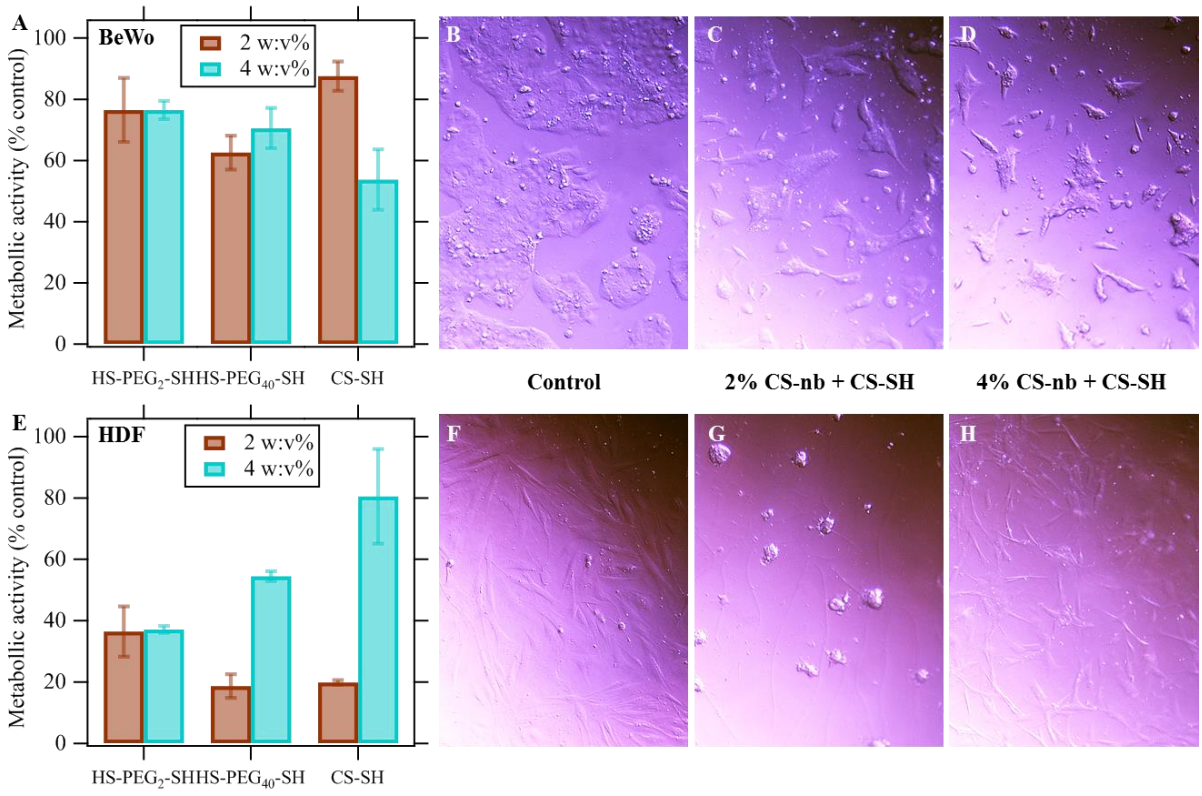

Figure 6. Cell viability relative to controls (100%) (A, E) and widefield microscopy images of BeWo (B-D) and HDF (F-H) cells 24 hrs after seeding on: the plate (B, F), CS-SH crosslinked 2 w:v% hydrogels (C, G) and CS-SH crosslinked 2 w:v% hydrogels with 0.25 w:v% collagen.

Although CS presents similarities with GAG in the ECM, its structure often fails to promote cell adhesion[52] and functionalisation with adhesion peptides such as RGD[53] hyaluronic acid,[54] or proteins (e.g. collagen (Col) [55] or gelatin[56, 57]) is common. The incorporation of Col (type I) into CS hydrogels (final concentration CS 2 w:v% - Col 0.25 w:v%) drastically improved HDF spreading and adhesion, resulting in viabilities greater than

90% for up to 6 days, while having minimum effect on BeWo (**Figure 7 and S6**). It is worth noting that only a small amount of Col was needed to significantly enhance cell adhesion, while Col hydrogels typically require concentrations higher than 0.5 w:v% to achieve a good viability[58]. Lower viabilities were generally observed when CS-SH was used as a crosslinker (**Figure 7**). The incorporation of Col into CS hydrogels had different impact on their rheological properties. While HS-PEG_{40}-SH crosslinked hydrogels presented similar *G*' values with and without Col, HS-PEG_2-SH substrates were slightly stiffer (*G*' ~ 1 to ~ 2 kPa) and CS-SH materials were drastically weaker (*G*' ~ 500 to ~ 80 Pa). SEM revealed that PEG crosslinked CS/Col hydrogels retained their honeycomb structure, with the presence of large, elongated and regularly spaced pores for HS-PEG_2-SH hydrogels and spherical ones for HS-PEG_{40}-SH materials. CS-SH crosslinked hybrids, however, presented a highly polydisperse structure, with the presence of numerous pores of smaller dimensions and random directions, as well as fibre-like regions, suggesting poor mixing between CS and Col (**Figure S7**). The interaction between Col and CS may prevent the formation of some crosslinks, especially with CS-SH where the thiol groups are very closed to the polymer backbone, and result in the smaller *G'* values obtained. In addition, interactions between charged groups of both polymers may reduce the crosslinking efficiency by hindering the nb moieties or increasing network inhomogeneity. These structural observations agree broadly with the rheology results, in which a loss in structural organisation related to poorer mechanical properties was noted. This also correlates with the observed cell viability, where both the presence of adhesive peptides of Col and high *G'* modulus and small mesh sizes (**Table S1**) were required to achieve efficient adhesion of HDF and good viabilities.

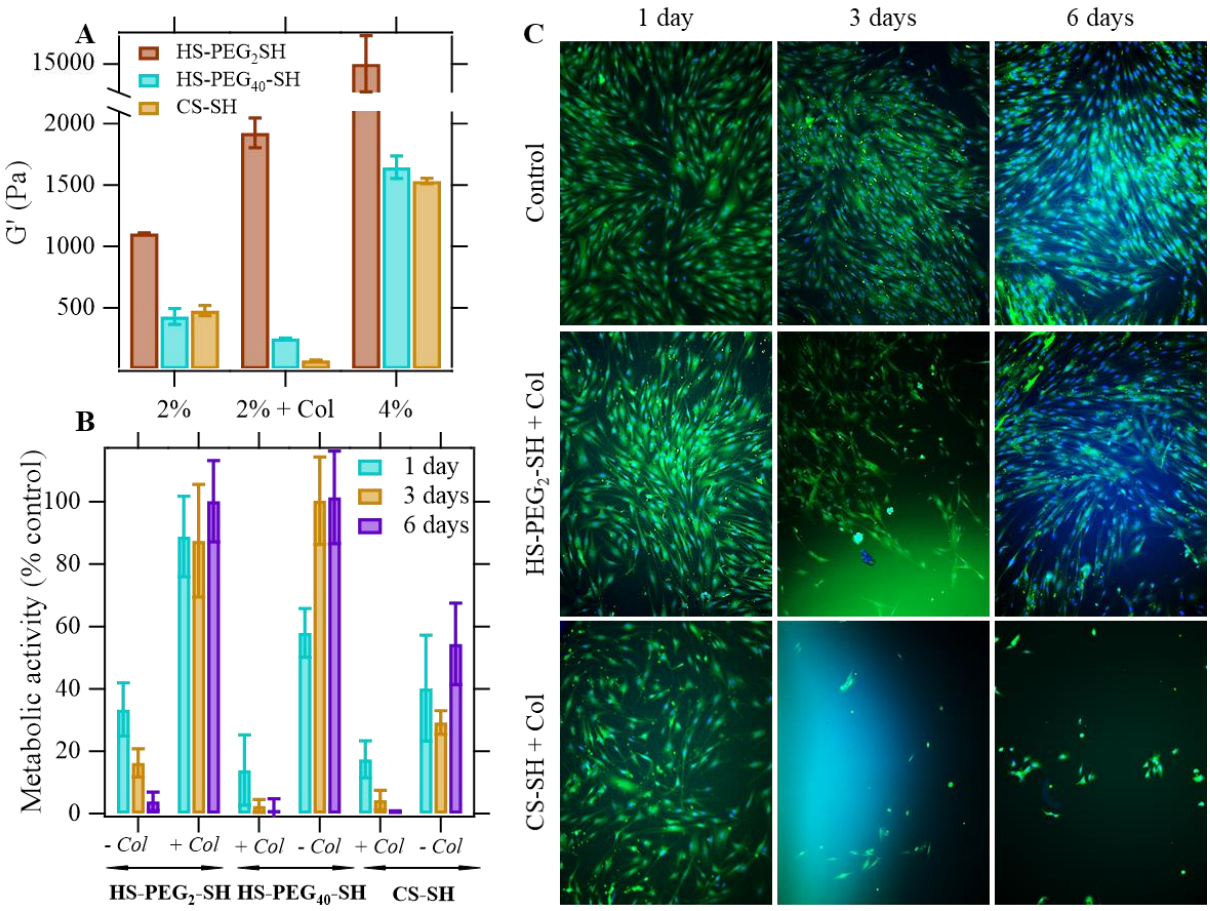

Figure 7. Characterisation of hydrogels investigated for cell studies. Rheological properties of all hydrogels cultured with HDF (A), metabolic activity (B), and widefield microscopy imaging of (C) cells after 1, 3 and 6 days of culture on CS hydrogels crosslinked with HS-PEG_2-SH or CS-SH, with or without 0.25 w:v% Col, compared to cells grown on plates (control).

Conclusion

In conclusion, a series of photo-crosslinked CS-based hydrogels were successfully synthesized by thiol-ene click reaction from a simple CS-nb precursor and different crosslinkers under UV exposure. The material properties could be readily tuned at the macro- and microscale by changing the crosslinking density, the nature of the crosslinker and the polymer concentration. The pore size dimensions, ranging between 20 – 100 µm and the rheological properties tuneable around 0.5 – 20 kPa were compatible with cells growth after addition of a low concentration of Col. Due to the fast gelation kinetics, hydrogels could be successfully generated *in situ* under dry and wet conditions and adhered to pork skin; could be molded into stable shapes; and could release entrapped compounds. All these conditions make CS-nb a potential candidate for biomedical applications in areas such as wound healing or tissue engineering. For future work, it would be interesting to characterise the tensile and

compression properties of hydrogels and correlate them with to cell viability and adhesion on the hydrogels.

Associated content

Supporting Information

The Supporting Information is available free of charge on the ACS Publications website at DOI: …. Detailed experimental procedures and characterization data (PDF)

Author information

Corresponding Authors

*E-mail: m.c.galan@bristol.ac.uk. Phone: +44 (0) 117-928- 7654.

*E-mail: wuge.briscoe@bristol.ac.uk; Phone: +44 (0)117 3318256

Author Contributions

S.M. performed all the experiments and data analysis. S.R. provided assistance on the SANS beamline. The manuscript was written through contributions of all authors, who also contributed to the data analysis and interpretation. All authors have given approval to the final version of the manuscript.

Notes

The authors declare no competing financial interest.

Acknowledgments

We thank Professor Craig Butts and Paul Lehman for help with the NMR and helpful discussions, Dr Margaret Saunders for providing the BeWo-b33 cells, Dr Jean-Charles Eloi for help and discussion with SEM. MCG and SM were supported by the European Research Council (ERC−COG: 648239) and the Bristol Chemical Synthesis Centre for Doctoral Training (Engineering and Physical Science Research Council (EPSRC) EP/L015366/1). This publication is based upon work from COST Action GLYCONanoPROBES (CA18132), supported by COST (European Cooperation in Science and Technology).

References

1. Zhu, J.; Marchant, R. E., Design properties of hydrogel tissue-engineering scaffolds. *Expert Rev. Med. Devices* **2011,** *8* (5), 607-626.

2. Guo, J. L.; Kim, Y. S.; Mikos, A. G., Biomacromolecules for Tissue Engineering: Emerging Biomimetic Strategies. *Biomacromolecules* **2019** 20, 8, 2904–2912

3. Guan, X.; Avci-Adali, M.; Alarçin, E.; Cheng, H.; Kashaf, S. S.; Li, Y.; Chawla, A.; Jang, H. L.; Khademhosseini, A., Development of hydrogels for regenerative engineering. *Biotechnol J* **2017**, 12, 1600394.
4. Beddoes, C. M. W., M.R.; Briscoe, W.H.; Su, B., Hydrogels as a Replacement Material for Damaged Articular Hyaline Cartilage. *Materials* **2016,** *9* 6 443 doi: 10.3390/ma9060443.
5. Xiang, J.; Shen, L.; Hong, Y., Status and future scope of hydrogels in wound healing: Synthesis, materials and evaluation. *Eur. Polym.* **2020,** *130*, 109609.
6. Radhakrishnan, J.; Subramanian, A.; Krishnan, U. M.; Sethuraman, S., Injectable and 3D Bioprinted Polysaccharide Hydrogels: From Cartilage to Osteochondral Tissue Engineering. *Biomacromolecules* **2017,** *18* (1), 1-26.
7. Khan, F.; Ahmad, S. R., Polysaccharides and Their Derivatives for Versatile Tissue Engineering Application. *Macromol. Biosci.* **2013,** *13* (4), 395-421.
8. Dragan, E. S.; Dinu, M. V., Polysaccharides constructed hydrogels as vehicles for proteins and peptides. A review. *Carbohydr Polym* **2019,** *225*, 115210.
9. Kasaai, M. R., Determination of the degree of N-acetylation for chitin and chitosan by various NMR spectroscopy techniques: A review. *Carbohydr Polym* **2010,** *79* (4), 801-810.
10. Croisier, F.; Jérôme, C., Chitosan-based biomaterials for tissue engineering. *Eur. Polym.* **2013,** *49* (4), 780-792.
11. Bernkop-Schnürch, A.; Dünnhaupt, S., Chitosan-based drug delivery systems. *Eur J Pharm Biopharm* **2012,** *81* (3), 463-469.
12. Bhattarai, N.; Gunn, J.; Zhang, M., Chitosan-based hydrogels for controlled, localized drug delivery. *Adv Drug Deliv Rev* **2010,** *62* (1), 83-99.
13. Sahariah, P.; Másson, M., Antimicrobial Chitosan and Chitosan Derivatives: A Review of the Structure–Activity Relationship. *Biomacromolecules* **2017,** *18* (11), 3846-3868.
14. Khan, F.; Pham, D. T. N.; Oloketuyi, S. F.; Manivasagan, P.; Oh, J.; Kim, Y.-M., Chitosan and their derivatives: Antibiofilm drugs against pathogenic bacteria. *Colloids Surf. B* **2020,** *185*, 110627.
15. Saporito, F.; Sandri, G.; Rossi, S.; Bonferoni, M. C.; Riva, F.; Malavasi, L.; Caramella, C.; Ferrari, F., Freeze dried chitosan acetate dressings with glycosaminoglycans and traxenamic acid. *Carbohydr Polym* **2018,** *184*, 408-417.
16. Peers, S.; Montembault, A.; Ladavière, C., Chitosan hydrogels for sustained drug delivery. *J Control Release* **2020,** *326*, 150-163.
17. Tiwari, S.; Patil, R.; Bahadur, P., Polysaccharide Based Scaffolds for Soft Tissue Engineering Applications. *Polymers* **2019,** *11* (1), 1 doi: 10.3390/polym11010001.
18. Boecker, A.; Daeschler, S. C.; Kneser, U.; Harhaus, L., Relevance and Recent Developments of Chitosan in Peripheral Nerve Surgery. *Front Cell Neurosci* **2019,** *13* (104) doi: 10.3389/fncel.2019.00104.
19. Ojeda-Hernández, D. D.; Canales-Aguirre, A. A.; Matias-Guiu, J.; Gomez-Pinedo, U.; Mateos-Díaz, J. C., Potential of Chitosan and Its Derivatives for Biomedical Applications in the Central Nervous System. *Front Bioeng Biotechnol* **2020,** *8* (389) https://doi.org/10.3389/fbioe.2020.00389.
20. Pei, M.; Mao, J.; Xu, W.; Zhou, Y.; Xiao, P., Photocrosslinkable chitosan hydrogels and their biomedical applications. *J. Polym. Sci. Part A: Polym. Chem.* **2019,** (doi:10.1002/pola.29305), 41563-41574.
21. Fairbanks, B. D.; Love, D. M.; Bowman, C. N., Efficient Polymer-Polymer Conjugation via Thiol-ene Click Reaction. *Macromol Chem Phys* **2017,** *218* (18), 1700073
22. Hoyle, C. E.; Lee, T. Y.; Roper, T., Thiol–enes: Chemistry of the past with promise for the future. *J. Polym. Sci. A Polym. Chem* **2004,** *42* (21), 5301-5338.

23. Wang, Z.; Jin, X.; Dai, R.; Holzman, J. F.; Kim, K., An ultrafast hydrogel photocrosslinking method for direct laser bioprinting. *RSC Advances* **2016,** *6* (25), 21099-21104.
24. Shih, H.; Lin, C.-C., Visible-Light-Mediated Thiol-Ene Hydrogelation Using Eosin-Y as the Only Photoinitiator. *Macromolecul Rapid Commun* **2013,** *34* (3), 269-273.
25. Lee, H. J.; Fernandes-Cunha, G. M.; Myung, D., In situ-forming hyaluronic acid hydrogel through visible light-induced thiol-ene reaction. *React Funct Polym* **2018,** *131*, 29-35.
26. Michel, S. E. S.; Dutertre, F.; Denbow, M. L.; Galan, M. C.; Briscoe, W. H., Facile Synthesis of Chitosan-Based Hydrogels and Microgels through Thiol–Ene Photoclick Cross-Linking. *ACS Appl Bio Mater* **2019,** *2* (8), 3257-3268.
27. Michel, S. S. E.; Kilner, A.; Eloi, J.-C.; Rogers, S. E.; Briscoe, W. H.; Galan, M. C., Norbornene-Functionalized Chitosan Hydrogels and Microgels via Unprecedented Photoinitiated Self-Assembly for Potential Biomedical Applications. *ACS Appl Bio Mater* **2020,** *3* (8), 5253-5262.
28. Bernkop-Schnürch, A.; Hornof, M.; Zoidl, T., Thiolated polymers—thiomers: synthesis and in vitro evaluation of chitosan–2-iminothiolane conjugates. *Int J Pharm* **2003,** *260* (2), 229-237.
29. Qu, X.; Wirsén, A.; Albertsson, A. C., Novel pH-sensitive chitosan hydrogels: swelling behavior and states of water. *Polymer* **2000,** *41* (12), 4589-4598.
30. Zhu, L.; Bratlie, K. M., pH sensitive methacrylated chitosan hydrogels with tunable physical and chemical properties. *Biochem Eng J* **2018,** *132*, 38-46.
31. Chang, C.; He, M.; Zhou, J.; Zhang, L., Swelling Behaviors of pH- and Salt-Responsive Cellulose-Based Hydrogels. *Macromolecules* **2011,** *44* (6), 1642-1648.
32. Gramlich, W. M.; Kim, I. L.; Burdick, J. A., Synthesis and orthogonal photopatterning of hyaluronic acid hydrogels with thiol-norbornene chemistry. *Biomaterials* **2013,** *34* (38), 9803-11.
33. Lee, S.; Park, Y. H.; Ki, C. S., Fabrication of PEG-carboxymethylcellulose hydrogel by thiol-norbornene photo-click chemistry. *Int J Biol Macromol* **2016,** *83*, 1-8.
34. McOscar, T. V. C.; Gramlich, W. M. J. C., Hydrogels from norbornene-functionalized carboxymethyl cellulose using a UV-initiated thiol-ene click reaction. *Cellulose* **2018,** *25* (11), 6531-6545.
35. Gomes, C.; Dias, R. C. S.; Costa, M. R. P. F. N., Static Light Scattering Monitoring and Kinetic Modeling of Polyacrylamide Hydrogel Synthesis. *Processes* **2019,** *7* (4), 237 https://doi.org/10.3390/pr7040237.
36. Chalal, M.; Ehrburger-Dolle, F.; Morfin, I.; Bley, F.; Aguilar de Armas, M.-R.; López Donaire, M.-L.; San Roman, J.; Bölgen, N.; Pişkin, E.; Ziane, O.; Casalegno, R., SAXS Investigation of the Effect of Temperature on the Multiscale Structure of a Macroporous Poly(N-isopropylacrylamide) Gel. *Macromolecules* **2010,** *43* (4), 2009-2017.
37. Hammouda, B.; Ho, D. L.; Kline, S., Insight into Clustering in Poly(ethylene oxide) Solutions. *Macromolecules* **2004,** *37* (18), 6932-6937.
38. Saffer, E. M.; Lackey, M. A.; Griffin, D. M.; Kishore, S.; Tew, G. N.; Bhatia, S. R., SANS study of highly resilient poly(ethylene glycol) hydrogels. *Soft Matter* **2014,** *10* (12), 1905-1916.
39. Horkay, F.; Hecht, A. M.; Mallam, S.; Geissler, E.; Rennie, A. R., Macroscopic and microscopic thermodynamic observations in swollen poly(vinyl acetate) networks. *Macromolecules* **1991,** *24* (10), 2896-2902.
40. Hyland, L. L.; Taraban, M. B.; Feng, Y.; Hammouda, B.; Yu, Y. B., Viscoelastic properties and nanoscale structures of composite oligopeptide-polysaccharide hydrogels. *Biopolymers* **2012,** *97* (3), 177-88.

41. Hung, K.-C.; Jeng, U. S.; Hsu, S.-h., Fractal Structure of Hydrogels Modulates Stem Cell Behavior. *ACS Macro Letters* **2015,** *4* (9), 1056-1061.
42. Li, X.; Katsanevakis, E.; Liu, X.; Zhang, N.; Wen, X., Engineering neural stem cell fates with hydrogel design for central nervous system regeneration. *Prog Polym Sci* **2012,** *37* (8), 1105-1129.
43. Ghobril, C.; Grinstaff, M. W., The chemistry and engineering of polymeric hydrogel adhesives for wound closure: a tutorial. *Chem Soc Rev* **2015,** *44* (7), 1820-1835.
44. Zavada, S. R.; McHardy, N. R.; Scott, T. F., Oxygen-Mediated Enzymatic Polymerization of Thiol-Ene Hydrogels. *J Mater Chem B* **2014,** *2* (17), 2598-2605.
45. Gupta, A.; Kowalczuk, M.; Heaselgrave, W.; Britland, S. T.; Martin, C.; Radecka, I., The production and application of hydrogels for wound management: A review. *Eur Polym J* **2019,** *111*, 134-151.
46. Zhou, Y.; Zhao, S.; Zhang, C.; Liang, K.; Li, J.; Yang, H.; Gu, S.; Bai, Z.; Ye, D.; Xu, W., Photopolymerized maleilated chitosan/thiol-terminated poly (vinyl alcohol) hydrogels as potential tissue engineering scaffolds. *Carbohydr Polym* **2018,** *184*, 383-389.
47. Moore, A. L.; Marshall, C. D.; Barnes, L. A.; Murphy, M. P.; Ransom, R. C.; Longaker, M. T., Scarless wound healing: Transitioning from fetal research to regenerative healing. *Wiley Interdiscip Rev Dev Biol* **2018,** *7* (2), 309.
48. Achterberg, V. F.; Buscemi, L.; Diekmann, H.; Smith-Clerc, J.; Schwengler, H.; Meister, J.-J.; Wenck, H.; Gallinat, S.; Hinz, B., The Nano-Scale Mechanical Properties of the Extracellular Matrix Regulate Dermal Fibroblast Function. *J Invest Dermatol***2014,** *134* (7), 1862-1872.
49. Correia Carreira, S.; Cartwright, L.; Mathiesen, L.; Knudsen, L. E.; Saunders, M., Studying placental transfer of highly purified non-dioxin-like PCBs in two models of the placental barrier. *Placenta* **2011,** *32* (3), 283-291.
50. Çolak, A.; Li, B.; Blass, J.; Koynov, K.; del Campo, A.; Bennewitz, R., The mechanics of single cross-links which mediate cell attachment at a hydrogel surface. *Nanoscale* **2019,** *11* (24), 11596-11604.
51. Hersel, U.; Dahmen, C.; Kessler, H., RGD modified polymers: biomaterials for stimulated cell adhesion and beyond. *Biomaterials* **2003,** *24* (24), 4385-4415.
52. Jiang, Y.; Deng, Y.; Tu, Y.; Ay, B.; Sun, X.; Li, Y.; Wang, X.; Chen, X.; Zhang, L., Chitosan-based asymmetric topological membranes with cell-like features for healthcare applications. *J Mater Chem B* **2019,** *7* (16), 2634-2642.
53. Park, K. M.; Joung, Y. K.; Park, K. D.; Lee, S. Y.; Lee, M. C. J. M. R., RGD-Conjugated chitosan-pluronic hydrogels as a cell supported scaffold for articular cartilage regeneration. *Macromol Res* **2008,** *16* (6), 517-523.
54. Deng, Y.; Ren, J.; Chen, G.; Li, G.; Wu, X.; Wang, G.; Gu, G.; Li, J., Injectable in situ cross-linking chitosan-hyaluronic acid based hydrogels for abdominal tissue regeneration. *Sci Rep* **2017,** *7* (1), 2699.
55. Reyna-Urrutia, V. A.; Mata-Haro, V.; Cauich-Rodriguez, J. V.; Herrera-Kao, W. A.; Cervantes-Uc, J. M., Effect of two crosslinking methods on the physicochemical and biological properties of the collagen-chitosan scaffolds. *Eur Polym J* **2019,** *117*, 424-433.
56. da Silva, M. A.; Bode, F.; Drake, A. F.; Goldoni, S.; Stevens, M. M.; Dreiss, C. A., Enzymatically Cross-Linked Gelatin/Chitosan Hydrogels: Tuning Gel Properties and Cellular Response. *Macromol Biosci* **2014,** *14* (6), 817-830.
57. Luo, X.; Liu, Y.; Pang, J.; Bi, S.; Zhou, Z.; Lu, Z.; Feng, C.; Chen, X.; Kong, M., Thermo/photo dual-crosslinking chitosan-gelatin methacrylate hydrogel with controlled shrinking property for contraction fabrication. *Carbohydr Polym* **2020,** *236*, 116067.

58. Yang, H.; Shen, L.; Bu, H.; Li, G., Stable and biocompatible hydrogel composites based on collagen and dialdehyde carboxymethyl cellulose in a biphasic solvent system. *Carbohydr Polym* **2019,** *222*, 114974.